END
DATE
FILMED

8 81

DTIC

②

FOREIGN TECHNOLOGY DIVISION
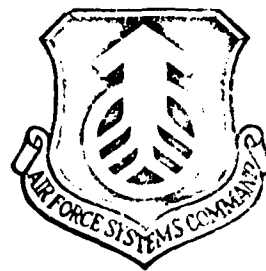
ACTA MECHANICA SINICA
(Selected Articles)

DTIC
SELECTED
JUL 29 1981

AD A102103

DTIC FILE COPY

81 7 28 047

EDITED TRANSLATION

FTD-ID(RS)T-0414-81   1 July 1981

MICROFICHE NR: FTD-C-81-000598

ACTA MECHANICA SINICA (Selected Articles)

English pages: 32

Source: Acta Mechanica Sinica, Nr. 3, 1978,
pp. 219-225, 230-237
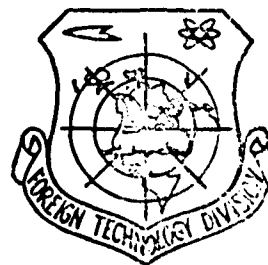
Country of origin: China
Translated by: SCITRAN
                F33657-78-D-0619
Requester: FTD/TQTA
Approved for public release; distribution
unlimited.

TABLE OF CONTENTS

EXPERIMENTAL TECHNIQUES AND METHODS

PRINCIPLE OF OPERATION AND MEASUREMENT ACCURACY OF MODEL YYB1-1 REMOTE STRAIN GAUGE

Ch'ung Ch'ing University   Fan Ching Hung

As the mechanics industry strides forward in the direction
of high speed,accuracy and high volume,the problem of strength,
vibration and hardness of the rotating parts of all kinds of
machines suddenly becomes very important.At home and abroad,
current collecting rings are generally used to bring out signals
for the purpose of measuring physical parameters of the rotating
parts.With such contact-type measurements,the amount of work done
is large,and the contact resistance between the current collector
and the brush is difficult to stabilize.This is why it has been
long conceived that one could employ a signal transmitter installed
on the rotating part to transform physical parameters such as strain
into electrical signals and use electromagnetic waves to carry these
signals onto the receiver,thus fulfilling the requirements of non-
contact type measurement.However,such remote strain gauges are
usually required to work under unfavorable conditions,especially so
in view of the weakness of the signals generated by the strain(on
the order of a few μV) and the serious electromagnetic interference
coming from the electric sparks and operating frequencies in the
industrial environment.In addition,space for installing gauges on
the rotating parts is usually very limited.This is why for a long
period of time no good solution has been found for such problems as
interference resistance,reliability,stability,accuracy and microni-
zation of the remote strain gauge.Aiming at solving this problem,

the Strain Remote Measurement Study Group of our university has
successfully fabricated the Model YYB1-1 Remote Strain Gauge(See
Plate I Photo 1)with the help of Ch'ung Ch'ing Steel Company,Tung
Fang Electrical and Machinery Factory,Hu Hsin Instruments Company
and Ch'eng Tu Academy of Communications Engineering.

I.Characteristics and Principle of Operation of the Remote Gauge

In our design,we have adopted electric field coupling and a
lower frequency range instead of the usual ultrashort waves for signal
transmission.Thus we were able to avoid the strong absoption by
metallic material of ultrashort waves,to simplify the circuit design,
and increase the reliability and stability of the system.Also,micron-
ization was facilitated by the elimination of the inductive elements
necessary for ultrshort waves.Pulse frequency modulation was used
instead of a sinusoidal regime.This increased the system's resistance
to interferences.Direct supply bridge was used to circumvent the
problem of distributive capacitance(which sometimes becomes more
significant in performing measurements on rotating parts).Circuit [1]
complexity and the necessity for using capacitance balancing poten-
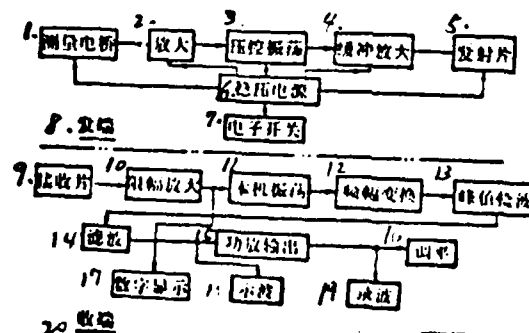tiometer were also avoided.Figure 1 shows a block diagram of the
circuit.

Fig.1 Block diagram of Model YYB1-1 Remote Strain Gauge
(Key, next page)

1. Measuring bridge
2. Amplifier
3. Pressure-regulated oscillator
4. Buffer amplification
5. Emitting plate
6. Constant voltage source
7. Electronic switch
8. Emission end
9. Receiving plate
10. Amplifier discriminator
11. Oscillator
12. Frequency-amplitude converter
13. Peak amplitude detector
14. Filter
15. Power amplifier
16. Balancing stage
17. Digital display
18. Oscilloscope
19. Recorder
20. Receiving end

On the signal emission end, variation in strain passes through the measuring bridge and is transformed into voltage variation. This is amplified and used to control a pressure-regulated oscillator. In this manner, variation in strain modulates the frequency of the rectangular pulses, and the train of pulses act as carrier of the desired strain signal. Such signals reach the receiving end via electric field coupling between the emitting plate and the receiving plate, and non-contact transmission of signal is achieved.

On the receiving end, owing to losses and external inteference incurred in the process of transmission, the pulse trains transmitted through the electric field are reduced in amplitude, distorted in shape and contain noises. To eliminate these effects, we let the signal pass through an amplifier discriminator so as to have sufficient output amplitude, and to restore the original shape of the pulse train. Then the signals were fed into a digital frequency counter to ascertain their static or average value of strain. The modified pulse train was passed through a frequency-amplitude converter, a rectifier and a filter. The digital signal(pulse frequency) was converted back into analog signal(strain waveform) and either recorded with crystal

oscillator oscilloscope or displayed on cathode ray oscilloscope.

Following is an analysis of the various parts of the remote gauge.

The Emission End

Constant voltage source — Variation in source voltage has decided effects on such parts as the bridge circuit. Owing to limitation on volume, the volume of the battery used on the emission end is generally small, and the decrease in voltage with time is significant (Fig.5). If electricity is supplied externally, then there will be larger variation in the source voltage that is coupled to the axle due to variation in the spacing between the axle and the source. Therefore, to ensure accuracy of the remote gauge measurements, it is very important to design higher-accuracy constant voltage source on the emission end. The difficulty involved lies not only in increased volume of the emission end but, more significantly, also in the higher currents required. This in turn reduces the life of the battery. (A set of high-accuracy constant voltage source uses approximately 10 mA of auxiliary current while the emission end itself only uses up 20-30 mA.) In our design, we made the bridge part of the constant voltage source, and used a series-type constant voltage source that contained feed-back loops so that the remote gauge used only about 3 mA of auxiliary current while it got the benefit of two sets of higher-accuracy constant voltage source. (For the positive source, variation in input voltage was 10%, while that for the output voltage was .1%; for the negative source, variation in input voltage was 10%, while that for the output voltage was 1%.)

The bridge — The sensing element consists of a common resistor-type or foil-type strain plate (Inner bridge uses two 120 Ω standard resis-tors) connected according to the general principle of strain measure-

ment into single arm,double arm and complete bridge strain measuring Wheatstone bridge circuits.If the corresponding resistor-type sensor was used, the bridge could be used for measuring speed,acceleration, pressure and other quantities.As only direct current was used,no capacitance balancing loops were required.If a potentiometer was used on the bridge to balance the resistors,then approximately 2% error would result because the resistance of the potentiometer would be on the bridge but would not respond to the variation in the signal.Taking into consideration the fact that the emission end of the remote gauge lies very close to the strain plate,one only needs to make careful choice of the resistance of the strain plate so that there exists only a very small nonlinearity. .Therefore,we have adopted unbalanced input on the bridge,and the operating point has been set with the help of the potentiometer in the amplifier.

Amplifier—The emission end of the remote gauge uses as its amplifier a linear integrated circuit.Different ranges of measurement are obtained by varying its closed-loop feed-back resitance which determines the amplification power.

Pressure-regulated oscillator — The function of the pressure-regulated oscillator is to transform pressure variation due to variation in strain into variation in frequency,thus achieving frequency modulation.This type of oscillators arise from multi-harmonic oscillators.They can generate pulse trains continuously.The frequency of the oscilloscope is controlled by the output voltage of the amplifier.Within the range of operation,linearity in pressure and frequency is preserved.This has been predicted by theory and borne out by experiments.

Buffer amplifier— Besides amplification of the oscillation,the main

function of the buffer amplifier is to isolate the oscillator from its surroundings so as to reduce parasitic frequency modulation.

Electronic switch— For measurements made on machinery that cannot conveniently be stopped,eg. a moving ship,the remote gauge has a simple electronic switch with the help of which one can control the switching of the power source at the emission end from the receiving end.The switch is connected to the base of the emission end switching crystal.When the switch for emission end power source,located at the receiving end,is in the off position,there is no potential on the base of the switching crystal.The crystal becomes nonconducting,the constant voltage source is cut off and no work is done by the emission end. When the switch is in the on position,current flows through the brush, the switch ring attains ground potential and the switching crystal becomes saturated.The constant voltage circuit is closed,and the emission end starts operating.In order to avoid problems arising from poor contact between the brush and the switch ring,we have designed a RC time-delayed return circuit,so that when the brush is temporarily disengaged from the switch ring,the emission end can still keep on operating normally.

The Receiving End

Impedance transformer— We have installed an impedance transformer on the receiving plate.This is an emitter-follower.It has a large input impedance,and can accept weak signals,thus increasing the allowable transmission distance.On the other hand,its output impedance is very low,so that it is allowed to have a very long cable and not suffer from interference.

Amplifier discriminator— To eliminate interference,we designed a two-terminal amplifier discriminator that has high-gain negative

feed-back.The noise waves entering through the receiving antenna are discarded by the discriminator after amplification,and the signal is restored to better defined square waves.

Main oscillator — This is a multi-harmonic oscillator with improved rising edge..

Its natural frequency of oscillation equals the central frequency designed.As the potential of the base is controlled by the amplifier discriminator,when the emission end is operating,the frequency of oscillation is forced to synchronize with the emission end.However, when the emission end is not operating,the frequency of oscillation becomes the central frequency.The oscillator has three functions:When the emission end suddenly has a power outage,the crystal oscillator will be protected;it indicates the regulation of the potentiometer on the emission end;it further improves the waveform of the pulse train.

Frequency-amplitude converter — Its function is to recover the freque modulated signal. The remote gauge adopts a self-sustaining saw-tooth wave circuit.The rectangular wave is transformed into a saw-tooth wave.The amplitude of the saw-tooth wave is inversely proportional to the frequency so that frequency-amplitude conversion can be achieved.

Peak-amplitude detection and filtering — The purpose of peak-amplitud detector is to obtain the envelope of the saw-tooth wave.The wave is first detected by a diode,and then passed through a RC filter,thus restoring the original strain waveform.

Power amplification — Power amplification is accomplished by using a two-stage cascade emitter-follower.Since the cascaded emitter-foll has a low output impedance,it can take a large load,and put out larg power.In order to have zero output of crystal oscillator when there

no strain,we have used a balancing stage,which is also made up of a two-stage cascade emitter-follower.A potentiometer is used to adjust the potential of the output so that the two ends of the crystal oscillator has zero potential difference.

II.Performance Tests And Chief Technical Indices of the Remote Strain Gauge

Linearity

Fig.2 shows the relationship between measured strain and output current.(The 'linear values' in the figure have been obtained by connecting full-scale point A to zero point with a straight line and finding the values on the ordinate corresponding to the given strain values.)In the measurement,the output terminal has a fixed load resistance.(This has been taken to be 15 Ω in accordance with the FC6-2500 crystal oscillator corresponding to Model SC-16 light ray oscilloscope.)For full-range output(set at 20 mA),error in linearity has been measured to be 1.35% for positive strain and 0.9% for negative strain.
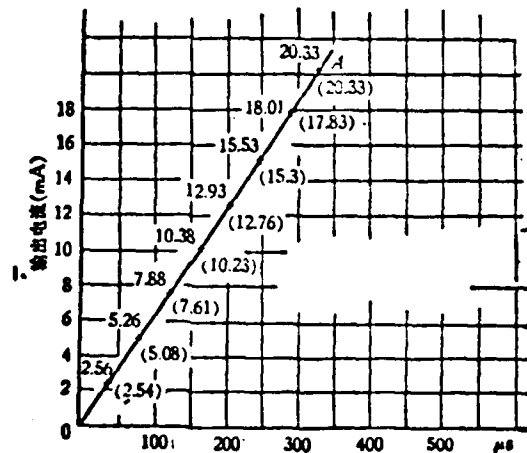

Fig.2 Strain at emission end vs.output current curve

Upper figures:average of 3 measurements

Lower figures:'linear values'

1. output terminal

Frequency Response

As a d.c. supply bridge is used, bridge circuit is purely resistive, and has no effect on the frequency response. One can open the bridge circuit to measure the frequency response characteristics of the instrument. A signal generator is used to input a constant amplitude sinusoidal wave at the emission end. After passing through the entire measurement system, the wave reaches the 15 Ω load. Fig.3 shows the variation with frequency of the voltage across the load. From this, one obtains an error of less than 3 % for frequency response when the frequency is 1000 Hz.
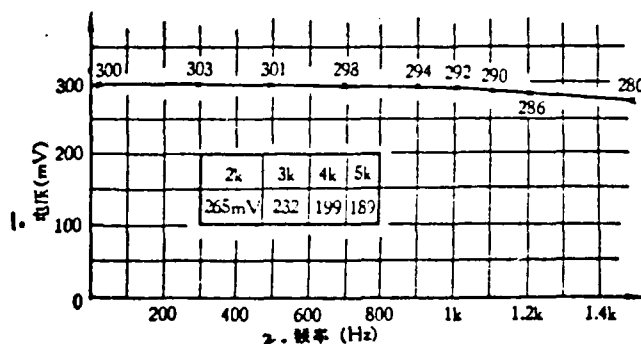
Fig.3 Frequency response curve

1. voltage

2. frequency

Stability

Stability with respect to receiving end source voltage fluctuation   We examined the effect on output of the input voltage at the emission end when the latter varied from 180 V to 242 V. The result is as shown in Fig.4. From the figure, it is obvious that the output of the receiver varies very little even for sizable fluctuation of the source voltage of the receiving end.

Instrument sensitivity drift.   Fig.5 shows the variation of the measured sensitivity and that of the emission end battery voltage as a function of time. One sees that although the battery voltage drops fairly rapidly, the sensitivity of the gauge varies only slightly with

time.(The batteries used are two sets of 6402-1 button batteries.)

Zero-point drift.   Zero-point drift curve is shown in Fig.6.From
the figure,one one can see that after 45 minutes warm-up time,the
zero-point drift is within 2% of the full scale over a period of
4 hours.
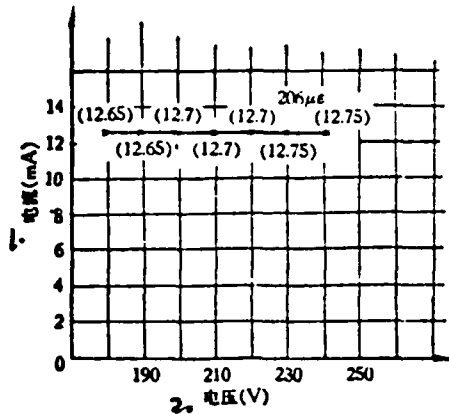
Fig.4 Receiver output current
　　vs. source voltage curve

1. Current

2.Voltage
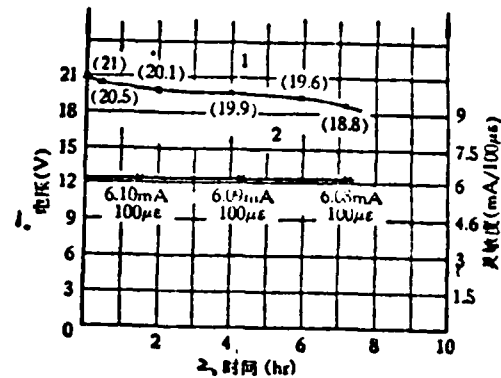
Fig.5 Curve 1:Variation of battery
　　　　　voltage with time

Curve 2:Variation of gauge
　　　　　sensitivity with time

1.Voltage

2. Time

Effect of Distance Between Emitting Plate And Receiving Plate

Fig.7 shows the variation of output cirrent with the distance
between the emitting and receiving plates under the condition of
constant strain.It is obvious that variation in distance has neglibl
effect on the accuracy of measurement.(When measuring strain of
rotating parts,the distance between the emitting and receiving plates
is usually from 20 to 200 mm.)
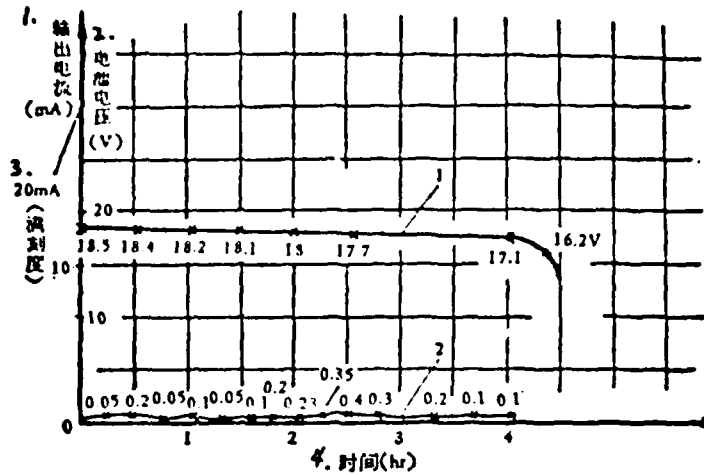
Fig.6 1)Curve showing drop in battery voltage when
battery was almost used up

2)Zero-point drift

1. Output current   3. Full scale

2. Battery voltage   4. Time

Fig.7 Variation of output current with distance
between emitting and receiving plates

1. Output current

2. Distance between emitting and receiving plates

Chief Technical Indices

Operating frequency:0-1000 Hz;error in frequency characteristics:

< 3%;maximum output current:(with 15 Ω load) ± 20 mA;error in
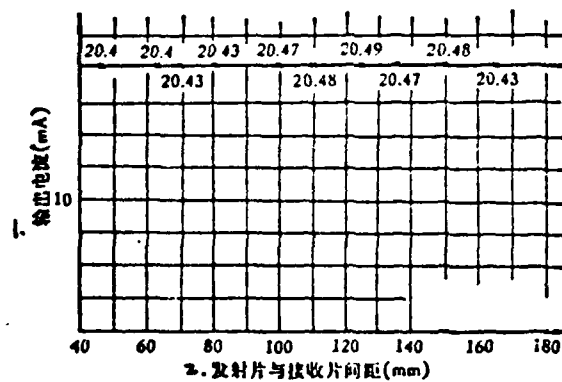linearity:(with 15 Ω load) < 1.5%;sensitivity:(with 15 Ω load) 0.05mA/
1 µε ;drift in sensitivity:± 2µε/hr;range of measurement:0-5000 µε
(6 ranges:± 300 µε;± 600 µε;± 1200 µε;± 2000 µε;± 3000 µε;± 5000 µε);
long cable transmission range: < 100m.

III. Rotary- -Bending Method for Testing Accuracy of Model YYB1-1
   Remote Strain Gauge

To test the accuracy of the remote strain gauge,the usual method
is to obtain two sets of signals from the vibrating beam,pass them
through the remote strain gauge and a common strain gauge respectively
and compare the results of measurement.Such methods do not take into
account the effects of rotation.Under rotating conditions,the
difficulty of testing the accuracy of the remote strain gauge lies in
the choice of a suitable standard strain signal.In order to overcome
this difficulty,we performed a rotary-bending measurement.(Plate I
Photo 2)

An axle was pushed against the pin on the lathe. A cantilever (Fig. 8a)
beam was placed on the axle and standard weights were bolted on an
end of the beam.When the axle rotates,the strain in the beam consists
of a constant strain resulting from centrifugal force,and a dynamic
strain caused by the action of weight W on the beam.The gravitational
component W_ρ of the beam bending caused by the latter can be express
as (Fig.8b)

$$W_\rho = W \sin \theta$$

Hence,theoretically,the dynamic strain must follow a sinusoidal curve.
Since the action of gravitational force on the beam should be the
same whether the beam is stationary or rotating at different speeds,
its amplitude can be found by using ordinary strain measuring devices
under static conditions.This is recorded as ε_0.As one can accurately

determine the weights of the standard weights and the bolt,the elastic modulus E of the beam and the location of the strain plate the theoretical value can be obtained by the following equation:

$$\varepsilon_t = \frac{M}{W \cdot E}$$

In the above equation,M is the bending moment at the center of the strain plate caused by the weight of the standard weights and the bolt;W is section modulus of the beam.
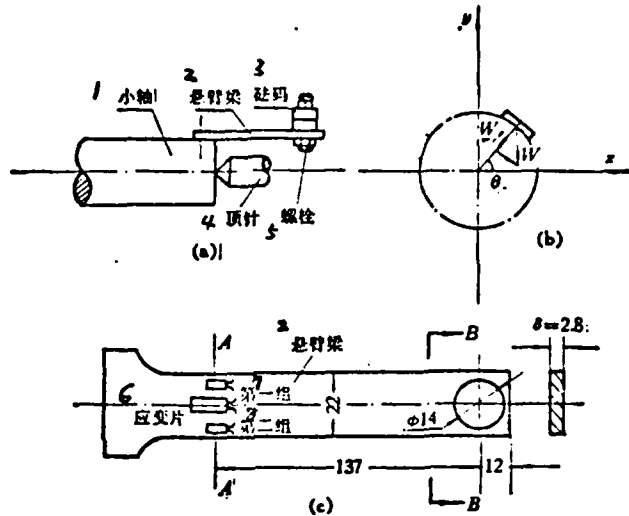
Fig.8 Rotary-bending measurement set-up

1.Small axle   5.Bolt

2.Cantilever beam 6.Strain plate

3.Standard weights 7.First set

4.Pushing pin   8.Second set

In order to increase the credibility of the results obtained the rotary-bending method,we simultaneously used a mercury current collecting ring.For comparison of waveforms,we connected the two se of strain plates located in plane AA of the beam (Fig. 8c) separate to Model YYB1-1 Strain Gauge and Current Collector-Model YJD1 Stra Measuring System,and took pictures of the waveforms simultaneously For comparison of strain amplitudes,we used the same set of short

moment strain plates for both the remote gauge and the current collector system.

The results of the comparison are shown on Plate I Photos 3-5. It is obvious that the waveform and phase are basically the same fo the two methods. The small ripples superimposed on the sinusoidal wave are due to the additional vibration of the beam caused by vibration of the lathe. (The lathe used in our measurement has low precision, hence the large bibration.) To obtain the strain amplitude ε_1 and ε_2 measured by the remote gauge and the current collector sys respectively, one should remove the ripples caused by vibration of t lathe. To do so, first enlarge the curve obtained from the oscillosco then connect the mid-points of the rising and falling edges of the ripples to obtain a smooth curve. This is the curve for the strain d to gravity. The vertical distance between the highest and lowest poi on this curve was measured separately on the scale ruled for the remote gauge and that for the current-collector system. The values obtained are 4 times the strain amplitude measured. (When the beam rotates from the highest point to the lowest point, the strain due to gravit changes sign, so that the measured value is twice the strain amplitu The other factor of 2 comes about bacause the two strain plates on the upper and lower sides of the beam are connected by a half-bridg Hence the total factor of 4. Similarly for the measured static value ε_0.)

Values for ε_0, ε_t, ε_1, ε_2 are tabulated in Table 1. The relati errors are with reference to the theoretically calculated value ε_t.

Table 1

1. 项 目	2. 应 变 值 *	3. 与计算值的相对误差
4. 静态测试	$\varepsilon_0 = 129\mu\varepsilon$	1.6%
5. 理论计算*	$\varepsilon_t = 127\mu\varepsilon$	—
6. 遥测应变仪测试	$\varepsilon_1 = 125\mu\varepsilon$	−1.6%
7. 集流环测试	$\varepsilon_2 = 131\mu\varepsilon$	3.1%

8* 弹性模量 E 约得为 $2.12\times10^6 kg/cm^2$.

(Key, next page)

1. Item

2. Strain value

3. Errors relative to calculated values

4. Measurement under static conditions

5. Theoretical calculation

6. Measurement using remote gauge

7. Measurement using current collector

8. Elastic modulus E was measured to be

In order to see if the remote gauge can work reliably on a long term basis under realistic unfavorable conditions,and how accurate the measured data are in an industrial environment,we tested the Model YYB1-1 Remote Gauge on the Model ϕ550 Shape Steel Rolling Mill of Ch'ung Ch'ing Steel Mill No.3.Our experiments show that the waveform of torque variation and that of freely decaying torsional vibration as measured by the remote gauge are basically the same as those obtained by the current-collector system.The curve on the oscilloscope is fairly smooth. These waveforms for torque and freely decaying torsial vibration of the axle system agree fully with those expected during shape steel milling.During the 40-hour continuous testing,40 sets of data were obtained for comparison,which showed that,basically,the values of torque measured by the two methods agree quantitatively also

Recently,we have successfully built a four-channel remote gauge. It has been applied to the experimental research on machine benches, and better results have been obtained.

REFERENCES

[1] Alen, A., Experimental Mechanics, 11, 8(1971).
[2] Joseph, V., Experimental Mechanics, 11, 12(1971).

THIN FILM RADIATIVE HEAT SENSOR

China Academy of Science,Mechanics Research Institute

Chu Nai I Li Hung Te Cheng Hui Liang Ts'ui Chi P'ing Li Lien Hs

Tien Chin University,Department of Radio Waves

Kao Chün Chieh Chang Jui Chih Tung Hsiang Hung Chang Min Huang

Wen Kuo

Thin film radiative heat sensor is a radiative heat measuring element that has simple construction,high sensitivity and fast respo It is especially suited for fast measurements on radiation in super-sonic equipment.It can also be employed in the calibration of radia energy.This type of sensor is made by covering the surface of an ordinary thin film resistance thermometer with a layer of carbon black[1-3],so as to increase its absorptivity,broaden the absorption spectrum,and reduce variation of absorptivity with wavelength.

In other countries,thin film radiative heat sensors have usuall been constructed by brushing specially prepared liquid metal suspens onto glass or ceramic substrates[4],or by covering the glass substrat sputtered with platinum film[5] with a previously prepared carbon fil Sensors made in this manner have inferior surface quality,and their frequency response curve only covers wavelengths below 1 μ.We have improved the construction technique by first sputtering a layer of platinum on the glass substrate,and then depositing the carbon direc onto the surface of the platinum film by means of vacuum deposition technique.The carbon film obtained this way has a better uniformity. One has better adhesion between the carbon film and the platinum fil In addition,the frequency response curve is extended to cover wave-
(Fig. 3
lengths below 2 μ,superior to similar sensors made in other countrie

1.Structure and Principle of Operation

Fig.1 shows the structure of the thin film radiative

heat sensor. The glass substrate has dimensions ϕ 20 mm x 5 mm, the platinum film is generally a few hundred Å thick, and the carbon film is usually from 1000 to 4000 Å thick. Because the carbon film is sufficiently thin, most of the radiative heat flow $\dot{q}_r$ transferred to it by external hot gases will be passed on to the platinum film[5]. Similarly, as the platinum film is sufficiently thin, its temperature will be representative of that of the glass substrate[3]. If a small current is applied to the platinum film via a silver wire, then when a constant external heat flow $\dot{q}_{r,f}$ impinges on the platinum film, its temperature and resistance will increase with time. Correspondingly, the voltage drop on the film will also increase. According to the theory of semi-infinite slab heat transfer, the temperature at the surface of the sensor has the following time dependence[6,7]:

$$T(t) - T(0) = q_{r,f} \cdot 2\sqrt{t/\pi(\kappa\rho c)} \text{ glass} \tag{1}$$

When a constant current I passes through the sensor,

$$T(t) - T(0) = \Delta V/I \cdot R_t \cdot \alpha \tag{2}$$

The relation between the voltage signal output of the thin film radiative heat sensor and heat flow (usually referred to as 'temperature curve') is given by

$$q_{r,f} = \frac{\sqrt{\pi(\kappa\rho c)_{glass}}}{2I \cdot R_t \cdot \alpha} \cdot \frac{\Delta V(t)}{\sqrt{t}} \tag{3}$$

The circuit used in our experiment is as shown in Figure 2. Hence, Equation (3) becomes

$$q_{r,f} = \frac{(R_0 + R_t)^2}{R_0 \cdot R_t \cdot E_0} \cdot \frac{\sqrt{\pi(\kappa\rho c)_{glass}}}{2\alpha} \cdot \frac{\Delta V(t)}{\sqrt{t}} \tag{4}$$

2. Fabrication Technique

A layer of platinum was first sputtered onto κ_9 glass using high vacuum film deposition equipment. The distance between the platinum target and the glass substrate was about 2.5 cm. Pressure inside the bell jar was 10^{-2} mm Hg. D.C. voltage was 1.2-1.5 kV. Current
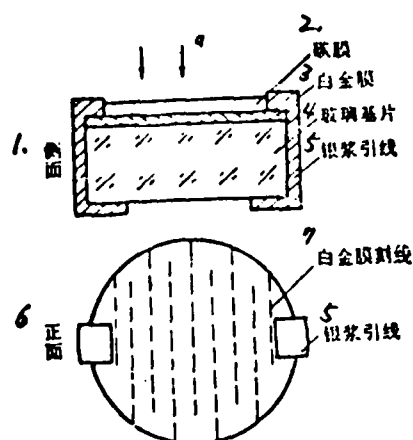
was 15-20 mA.Sputtering time was about 13 minutes.

Fig.1 Schematic diagram of thin film radiative heat sensor

1.Side-view

2.Carbon film

3.Platinum film

4.Glass substrate

5.Silver wire

6.Front-view

7.Rulings on platinum film
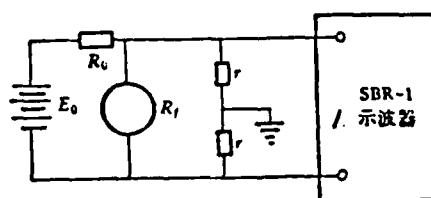
Fig.2 Circuit for measuring 'temperature curve'

1.Oscilloscope

To increase the resistance of the platinum film so as to obtain higher sensor sensitivity,we used a knife blade to make parallel rulings on the platinum film.The total resistance of the platinum film then became approximately 200-300 Ω .The sensor was then placed in a high temperature oven,heated to 610-630 $^\circ$C,kept at this temperature for 2 hours,and allowed to cool down gradually by itself.After annealing, the resistance dropped to 60-100 Ω .A carbon film was deposited on the platinum film by means of vacuum evaporation deposition technique.

Better results were usually obtained when two pairs of carbon electrodes were used. Vacuum had to be better than 5×10^{-5} mm Hg. The current was about 150 A. Evaporation time was about 2 seconds. Finally, aging was achieved by passing a current of several tens of mA through the sensor for 10 to 20 minutes. This was to enhance the stability of the sensor.

3. Calibration

Although the transmittance of a single layer of platinum film is generally smaller than 2%, the reflectance is as high as 40-60% and varies significantly with wavelength. A single layer of carbon has a reflectance of 10-20%, but its transmittance can also reach 10-20%. By employing the arrangement of a carbon film on top of a platinum film we have overcome the above difficulties. Fig.3 gives the variation with wavelength of the total transmittance, the total reflectance and the total absorptivity for the Type II sensor most often used in our experiments. One can see that in the wavelength range between $0.2\,\mu$ and $2.2\,\mu$. The total absorptivity of the sensor stays within the range $0.85 \pm 10\%$. In our experiments, we have approximated the total absoptivity to be 0.85. We measured the temperature dependence of the resistance of the platinum film in the range 24.4-$79.0\,^{\circ}$C, and the temperature coefficient was found found from $\alpha = (R_{T_2} - R_{T_1})/R_{T_1}(T_2 - T_1)$. The two Type II sensors used most often in our experiments both had $\alpha = 3.06 \times 10^{-3}$/degree. We examined the thickness of standard samples of carbon film on various models of sensors with Model 6J interference Microscope. Type II carbon film had a thickness of less than $1400\,\overset{\circ}{A}$. We also used JSM-U3 Scanning Electron Microscope to examine the surface features of standard carbon film samples. Magnification was increased from 60x to 30000x. Only a few black spots on the order of $1\,\mu$ were seen on the edges of the samples. These were probably gas bubbles or pin holes. The rest of the suface was smooth and flat,

showing good uniformity of the carbon film.

4. Experimental Methods and Set-Up

Eight cylindrical flat-head models with diameter r_3 = 29 mm were installed together in the Model 800 Excitation Tube of our laboratory. In the middle of the model head was a 5 mm thick quartz window with radius r_2 = 8 mm or 10 mm. The distance between the surface of the sensor and the outer surface of the window was usually about 6-8 mm. The effective radius of the surface of the sensor was 8 mm or 9.5 mm.

We assume that the gas flow in Region(2) of the tube was uniform during the effective period of the experiment. The radiative energy of the arc excited waves at the model head and that of the high temperature gas between the model windows was transmitted through the window and absorbed by the sensor. The voltage signal generated in the platinum film was displayed on the SBR-1 Oscilloscope. One can use Equation (4) to calculate the flow rate $q_{r,l}$ of radiative heat incident on the sensor.

Under our present experimental conditions, the high temperature gas at the model head is optically dilute. Let us further assume that the temperature and density are constant throughout the arc excited wave. Then, according to geometric allocation, under nodal-point conditions, the relation between the total radiative energy E of the high temperature gas and the flow rate $q_{r,l}$ of the radiative heat received by the sensor will be given by

$$q_{r,l} = {}^{1}F_q \cdot {}^{2}T_w \cdot a_l \cdot \delta \cdot {}^{3}F_A \cdot \frac{E}{2} \tag{5}$$

$$F_A = \frac{1}{2\pi \cdot s_1} \iint ds_1 \cdot \iint \frac{\cos\beta}{r^2} ds_3 \tag{6}$$

In our work, we have chosen F_{arc} = 1, T_{window} = 0.9, a_l = 0.85, δ/r_3 = 0.55, approximately. The geometric factors of the TypeII sensors used most often are F_g = 0.38 (#1) and 0.24 (#6).

At the same time,we measured the radiative heat transfer in
Region(5) under the conditions of reflected excitation wave.Namely,
a reflecting cylinder with 9.2 cm diameter and 8 cm depth was added to
the front of the model head.If one considers the rate of increase in
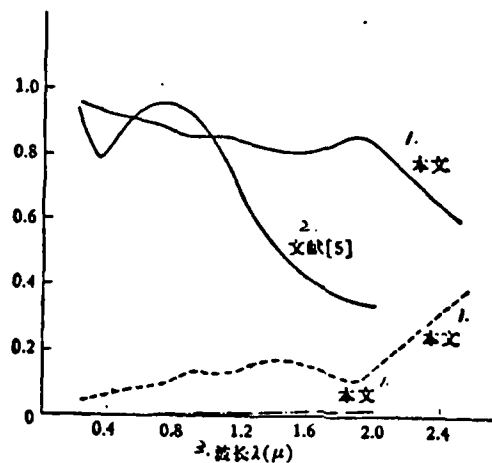
Fig.3　　Optical properties of Type II Thin Film Radiative

　　　　　Heat Sensor

　　　　　── absorptivity

　　　　　···· reflectance(MPS-5000 Monochromator Spectrometer)

　　　　　─·─ transmittance(Beckman Monochromator Spectrometer)

1.Present article
2.Ref.[5]
3.Wavelength

(illegible)

Fig.4 Comparison of theory and experiment for radiative

　　　　energy of high temperature air under equilibrium

　　　　conditions

1.Equivalent speed of flight　2.Experimental values

3.Theoretical values 4.Reference 5.Present article

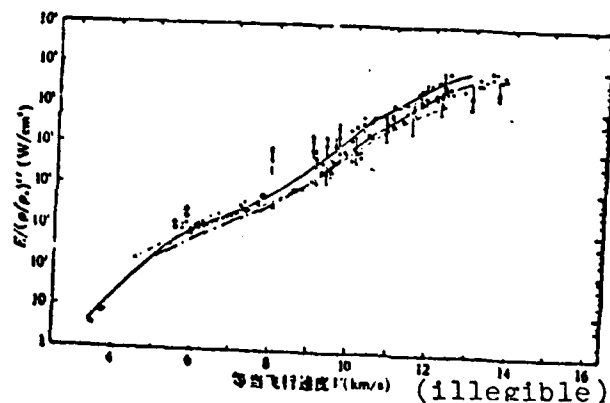the thickness of Region(5) to be approximately uniform,and the temperature and density of this region to be constant,then because the heat flow rate at the window and at the surface of the sensor is directly proportional to the thickness of Region(5),it will also be directly proportional to time:

$$q_{r,f}(t) = A \cdot t \tag{7}$$

After integration,the voltage signal generated at the surface of the sensor is found to be

$$\Delta V(t) = B \cdot t^{1/2} \tag{8}$$

Under constant voltage $\overset{E_0}{_{\wedge}}$conditions,Eq.(4) becomes

$$q_{r,f}(t) = \frac{3\pi}{4} \frac{(R_0 + R_f)^2}{R_0 \cdot R_f \cdot E_0} \cdot \frac{\sqrt{\pi(\kappa\rho c)}_{glass}}{2a} \cdot \frac{\Delta V(t)}{\sqrt{t}} \tag{9}$$

Correspondingly,Eq.(5) becomes

$$q_{r,f}(t) = F_3 \cdot T_w \cdot a_f \cdot \delta(t) F_\lambda \cdot \frac{E}{2} \tag{10}$$

where $\dot{q}_{r,f}(t)$ is the heat flow rate at time t; $\delta(t)$ is the thickness of Region(5) at time t;the other coefficients are the same as in Eq.(5)

5.Experimental Results

We obtained radiative heat flow rate repeatedly at the nodal point and in Region(5) under the three conditions p_1=10,1 and 10^{-1} mm Hg. The scatter of the testing points was generally within ± 20%.

A comparison of our experimental results with experimental result and theoretical calculations done abroad is given in Fig.4.The devia- tion of the average value we obtained from those obtained by others is generally within a few tens percent.This is on the same order of magnitude as the deviation of values among the results obtained by the other authors.The trend of variation with different conditions also agrees with that observed by other authors.This means that these data should be useful in practical engineering applications.

From the preliminary experimental results,it can be seen that our sensor meets the requirements on durability,sensitivity and

response time. Reproducibility and stability in repeated experiments are also good. Of course, fabrication is still crude and calibration is not yet complete. Experimental errors arose mainly from irreproducibility of experimental conditions and inaccuracy in the determination of the speed of the excitation wave. Other factors include calibration, non-uniformity of gas flow and presence of impurities. Improvements need to be made in the future.

We would like to extend our thanks to Comrade Shan Tse Chen who gave us a great deal of help with the platinum film sputtering.

REFERENCES

[1] W., Klaus, *The Review of Scientific Instruments*, 44, 1(1973), 23.
[2] Rose, P. H. and Stark, W. L., *J. Aero. Sci.*, 25, 2(1958), 86.
[3] Videl, R. J., A. R. S., TP-327 (1956).
[4] Nerem, R. M., AD-432473 (1964).
[5] Hoshizaki, H., AD-424935 (1963).
[6] Videl, R. J., Cornell Aeronautical Laboratory, Rep. AD-917-A-1 (1956).
[7] Carslow, H. S., Conduction of Heat in Solids (1959).
[8] Page, W. A., IAS, Paper 63—41 (1963).
[9] Nerem, R. M., AD-601371 (1964).
[10] Gruszczynski, J. S., *AIAA Paper 66-103* (1966).
[11] Golobic, R. A., *AIAA. J.*, 6, 9(1968), 1741.
[12] Kivel, B., AVCO. RR., 21(1957).
[13] Breene, R. G; Nardone, M. C., GE R62 SDS2 (1962); GE R63 SD3 (1963).
[14] Meyerott, R. E., LMSD. 288052 (1959); Geobysical Research, Paper 58, GRD-TN-60-277 (1960).

RESEARCH REPORT

DETERMINATION OF PARAMETERS OF MODEL Φ800 EXCITATION TUBE

China Academy of Science,Mechanics Research Institute

Chu Nai I   Li Hung Te Cheng Hui Liang   Li Lien Hsiang

!.Experimental Set-Up and Principle of Operation

In our experiment,a cylindrical stainless steel wave excitation tube was used.High voltage section has length 1.6 m and inner diameter 223 mm;low voltage and experimental region has inner diameter 800 mm. Hydrogen-oxygen combustion was used for driving.Driving pressure was about 80 ata.The effective distance between the measuring stand and the sensing film was about 14 m.

We used a thin-film-resistance-thermometer type [1] gold film heat sensor in the excitation tube to measure the length of Region(2) and the shape of the wavefront.The interface between the Intermediate Region and Region(3) was determined using an electric probe.These signals were fed directly or via a thermoelectric simulation circuit [into SBR-1 Oscilloscope.

When the excitation wave first arrives at the gold film,the heat flow carried by the high temperature gas causes the film temperature to rise abruptly.Hence,arrival of the wavefront is indicated by a sudden appearance of signal on the temperature curve or heat flow curve(after passing through the thermoelectric simulation circuit) recorded by the oscilloscope.After this comes Region(2) of uniform flow.Basically,the speed of heat flow from the high temperature gas to the gold film does not vary,and one obtains on the oscilloscope a smooth parabolic temperature curve or a horizontal heat flow curve. When the interface between the Intermediate Region and Region(2) arrives,because of the change in state of flow before and after the interface,one should see an obvious point of inflection on both the

temperature curve and the heat flow curve recorded by the oscillosco
Thus the appearance of signal and the point of inflection mark the
endpoints of the length of homogeneous flow of Region(2).

In order to measure the shape of the wavefront,we placed more
than two sensors on the same horizontal plane perpendicular to the
axis of the excitation tube,at various distances from the axis.To
avoid the problem of the two oscilloscope scanning beams being
unsymmetrical,we fed the signal from two sensors into the same
scanning beam,one with positive polarity and the other with negative
polarity.The signal thus recorded is a superposition of two gold film
temperature curves.When the wavefront reaches gold film #1 first,the
total signal rises rapidly and when the wavefront reaches gold film #
the total signal drops abruptly;conversely,if the wavefront reaches
gold film #2 first,the total signal first drops,then suddenly rises
when the wavefront reaches gold film #1.In this manner,one can
accurately determine order in which the wavefront reaches the gold
films.The distance between the two   points of change on
the total signal is simply the time difference between the arrival of
the wavefront at the two gold films.This,multiplied by the speed of
the excitation wave,gives the degree of bending of the wavefront
between the two positions.

In actual excitation tubes,the mass loss due to the presence of
the boundary layer and the turbulent mixing of the gases between
Region(2) and Region(3) result in a fairly long Intermediate Region.
As the gas in Region(3) is cold and contains no charged particles,
while the Intermediate Region contains some charged particles due to
mixing with the gas of Region(2),we were able to use an electric prob
to determine the location of the interface between the Intermediate
Region and Region(3).

2.Expermental Results

Based on the expermental results,the state of flow in the excitation tube can be qualitatively divided into several regions as shown in Fig.1.
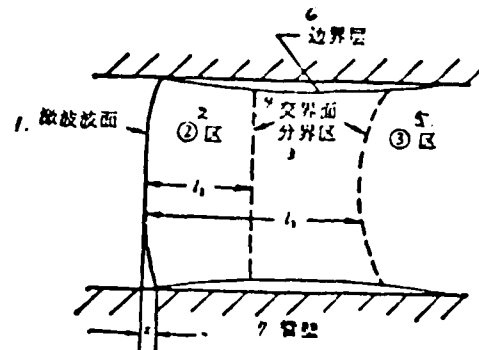

Fig.1 Schematic diagram of state of flow in the excitation tube

1.Wavefront   5.Region(3)

2.Region(2)   6.Boundary layer
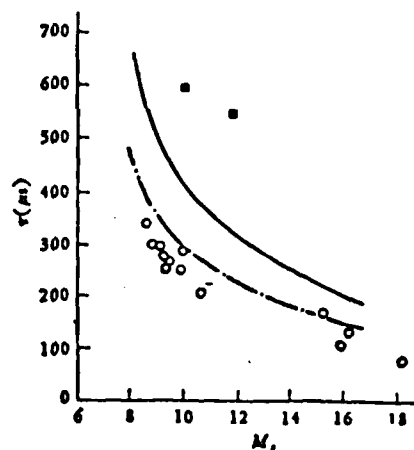
3.Intermediate Region   7.Tube wall

4.Interfaces

Fig.2 Determination of the location of the Intermediate Region

$p_1 =$ 1 mm Hg, $x_s =$ 14 m

o Interface between Region(2) and Intermediate Region as determined with heat sensor

■ Interface between Region(3) and Intermediate Region as determined with the electric probe

— Period of uniform flow in Region(2) of an ideal tube

—·—Period of uniform flow after Mirels correction for turbular flow[4]

Fig.3 Determination of the location of the Intermediate Region

$p_1 = 10^{-1}$ mm Hg, $x_s = 14$ m

X   Interface between Region(2) and the Intermediate Region as determined with heat sensor

■   Interface between Region(3) and Intermediate Region as determined with electric probe

—   Period of uniform flow in Region(2) of an ideal tube

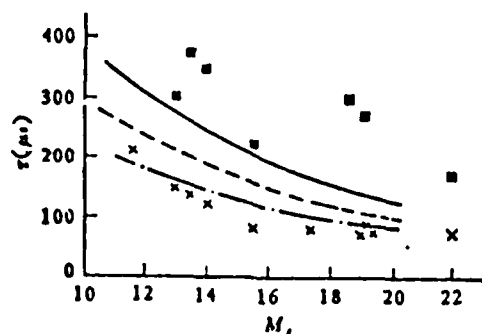--- Period of uniform flow after Mirels correction for laminar flow [3]

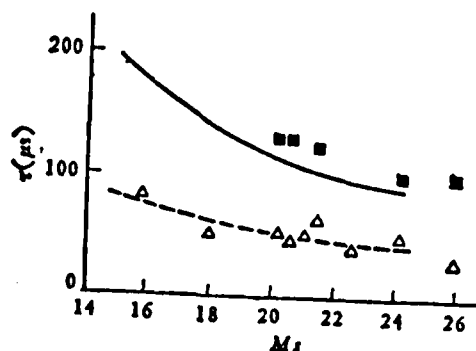—·— Period of uniform flow after Mirels correction for turbular flow [4]

Fig.4 Determination of the location of the Intermediate Region

$p_1 = 10^{-2}$ mm Hg, $x_s = 14$ m

△   Interface between Region(2) and the Intermediate Region as determined with heat sensor

■   Interface between Region(3) and the Intermediate Region as determined with the electric probe

—   Period of uniform flow in Region(2) of an ideal tube

--- Period of uniform flow after Mirels correction for laminar flow [3]

1)Length of Region(2)   Figs.2-4 give the length of time of uniform flow in Region(2).The trend of variation of τ_2 with M_s agrees with theoretical analysis.The value of τ_2 actually measured is usually only 1/2 to 2/3 that of the ideal excitation tube.This shows that loss at the boundary layer and mising at the first interface result in a substantial reduction of the effective period of uniform flow in Region(2) of the tube.

$p_1 = 1,\ 10^{-1},\ 10^{-1}\text{mmHg}$

Quite a few authors have studied and discussed the problem of length reduction of Region(2) due to the presence of the boundary layer in the excitation tube.Mirels' theory [3,4] is generally regarded as being more reliable.Comparing our experimental results with the theoretical values obtained after Mirels correction,we found that at $p_1 = 1$ mm Hg,the experimental points are a little lower than the curve corrected for boundary layer turbular flow;at $p_1 = 10^{-1}$ mm Hg, for high and low M_s,the experimental points fall between the curve corrected for laminar flow and that corrected for turbular flow, while for intermediate M_s values,the expermental points lie a little lower than the corrected curves;at $p_1 = 10^{-2}$ mm Hg,the experimental points agree fairly well with the curve corrected for laminar flow for the entire range of values of M_s.Our experimental results agree basically with those obtained by Lin Shau Chi et al[5] for their 24-inch excitation tube at $p_1 = 10^{-1}$ and 10^{-2} mm Hg.An observation worth mentioning is the tendency for the experimental results to agree better with the theoretical curve corrected for boundary layer laminar flow at lower p_1,and to agree better with the curve corrected for boundary layer turbular flow at higher p_1;a state of transition is exhibited for intermediate p_1.

In order to further study the variation of τ_2 with p_1,we measure the value of τ_2 corresponding to different p_1,holding M_s constant. The results for $M_s = 10$ and 15 are shown in Figs. 5 and 6.We see that

for $p_1 = 10^{-2}$ mm Hg or lower, τ_2 agrees with the value predicted by laminar flow theory, i.e. under this condition, the state of flow in the boundary layer of the tube is mainly laminar. For $p_1 = 1$ mm Hg or higher, τ_2 agrees with the value predicted by turbular flow theory, and is much lower than that predicted by the laminar flow theory. Under this condition, the state of flow in the boundary layer is mainly turbular. In both of these regions, τ_2 increases with p_1.

In the Intermediate Region, the contributions from neither the laminar flow nor the turbular flow should be neglected. As p_1 increases, the increase in τ_2 becomes smaller and there is even a drop in τ_2. This transition occurs

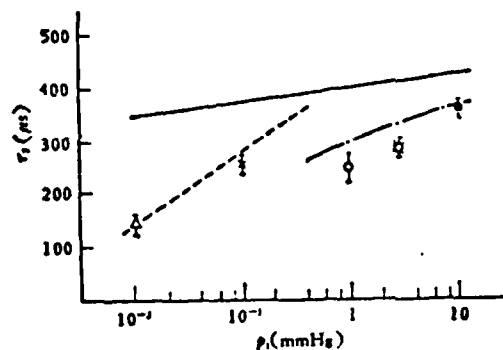approximately between 10^{-1} and 1 mm Hg for our excitation tube.

Fig.5 Variation of period of uniform flow in Region(2) with p_1
       $M_s = 10$, $x_s = 14m$

— Period of uniform flow in an ideal tube

— Period of uniform flow after Mirels correction for laminar
   flow

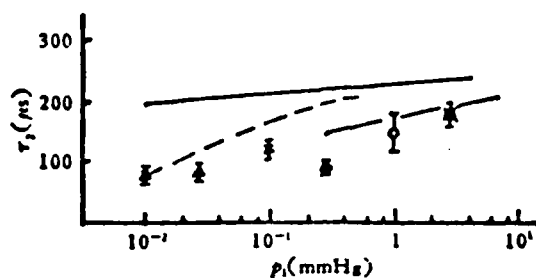—·— Period of uniform flow after Mirels correction for turbular
   flow

Fig.6 Variation of period of uniform flow in Region(2) with p_1

$M_s = 15$, $x_s = 14m$

—— Period of uniform flow in an ideal tube

—— Period of uniform flow after Mirels correction for laminar flow

—·— Period of uniform flow after Mirels correction for turbular flow

To examine the validity of the above viewpoint,we used gold-film heat sensors installed on the side wall of the excitation tube to determine the position l_t of the turning point in the boundary layer, and compared it with length $l_2 = \tau_2 \cdot u_2$ of Region(2) measured inside the tube.At $p_1 = 1$ mm Hg, $l_t \lesssim l_2/3$.(Under this condition,the Reynold number $Re_t = (W-1)^2 u_{e,o} \cdot \rho_{e,o} \cdot l_t/\mu_{e,o} \approx 2 \times 10^6$.)

This shows that the turning point lies far in front of the first interface.The flow in that part of the boundary layer corresponding to Region(2) is mainly in a turbular flow state.Hence,basically,we should use turbular theory to estimate the effect of loss on length reduction of Region(2).At $p_1 = 3 \times 10^{-2}$ mm Hg, $l_t > l_2$, the turning point is located behind the first interface,i.e. the flow in that part of the boundary layer corresponding to Region(2) is entirely in a laminar flow state.Therefore,one should use the laminar flow theory to estimate the effect of loss in the boundary layer on the reduction in length of Region(2).

2)Shape of the Wavefront

Fig 7 gives the results of measurement of wavefront under the conditions $p_1 = 1 \times 10^{-2} - 3 \times 10^{-2}$ mm Hg and $M_s = 20$. r denotes the

distance between the point of measurement and the axis of the tube; x denotes the difference in distance on the wavefront between the point of measurement and the center of the wavefront. Taking the center of the wavefront as the origin, we assign a positive value for lagging points on the wavefront and a negative value for leading points on the wavefront. The waveform distortion as measured by our experiment is on the   average   about 5 times as large as that calculated from existing boundary layer theories[6,7], and 2-3 times as large as the results obtained by Lin Shau Chi et al[5] .Near the wall, the average value of x/R is around 7%. This shows that the degree of wavefront distortion is quite large. However, in the region within a radius of 10 cm from the center, the wavefront is basically flat. When p_1 increases, unevenness of the wavefront decreases. In our set-up, the serious wavefront distortion may have been due to the larger inner diameter and the not sufficiently stable hydrogen-oxygen combustion drive.
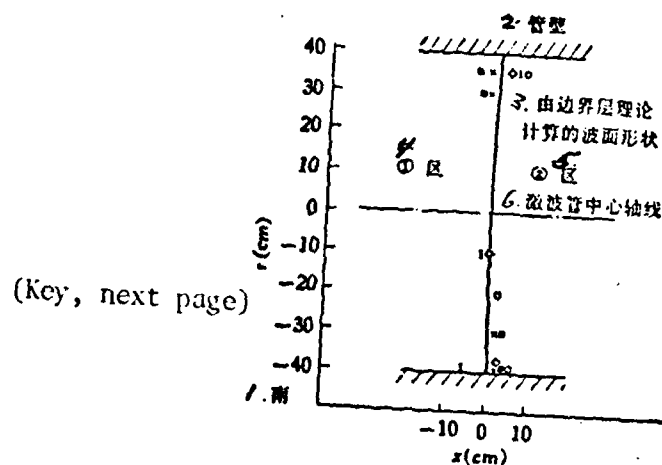
(Key, next page)

Fig.7 Experimental results of measurement of shape of wavefront

$M_s=20$, $p_1=(1-3) \times 10^{-2}$ mm Hg

Center of wavefront is taken as the origin.

■ , × , ✗ , I , o

represent 5 typical results of measurement

1.South
2.Wall
3.Shape of wavefront as calculated from boundary layer theory
4.Region(1)
5.Region(2)
6.Axis of tube

3) The Intermediate Region between Region(2) and Region(3)   Figs.
2-4 give the position l_2 or τ_2 of the interface between Region(2) and
the Intermediate Region as well as the position l_3 or τ_3 of the inter-
face between the Intermediate Region and Region(3). Roughly speaking,
τ_3 is about twice as large as τ_2 ,i.e. l_3 is twice as large as l_2.
In other words, the lengths of the Intermediate Region and Region(2)
are on the same order of magnitude. We compared the value of τ_3 we
obtained with an electric probe inside the tube with that obtained
previously by Comrades Tsui Chi P'ing et al who used an electric probe
to make measurements in the boundary layer at the tube wall. Under the
conditions $p_1=10^{-2}$ mmHg, $M_s=20$, $\tau_3 \cong 13C\,\mu s$ inside the tube while τ_3 is
approximately 400-500 μs along the tube wall. This shows that the
Intermediate Region is longer at the wall than inside the tube,
as is evident from Fig.1.

We would like to cordially thank Comrades Yü Hung Ju and Shan Tse
Chen who gave us valuable help in the use of the thermoelectric
simulation circuit and in the fabrication of the gold film heat sensor.

REFERENCES

[1] Rose, P. H. and Stark, W. I., J. Aero. Sci., 25, 2 (1958), 86.
[2] Meyer, R. F., N.R.C. of Canada Aero. Report, LR-375 (1963); Skinner, G. T., A. R. S. J., 30, 6(1960), 569.
[3] Mirels, H., Phys. Fluids, 6, 9(1963), 1201.
[4] Mirels, H., AIAA J., 2, 1(1964), 84.
[5] Lin, S. C. and Frie, W. I., Phys. Fluids, 4, 2(1961), 238.
[6] Hartunian, R. A., Phys. Fluids, 4, 9(1961), 1059.
[7] De Boer, P.C.T., Phys. Fluids, 6, 7(1963), 962.